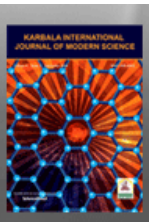

Karbala International Journal of Modern Science

Volume 8 | Issue 2 Article 5

# Structural and Spectroscopic Analysis for Silver Bulk and Nanoparticles

Hajir M. Fadhil
*Department of Applied Science, University of Technology, Baghdad, Iraq.*, hajirmohammed66@gmail.com

Khaleel I. Hassoon
*Department of Applied Science, University of Technology, Baghdad, Iraq.*

Hyder A. Salih
*Department of Applied Science, University of Technology, Baghdad, Iraq.*

Follow this and additional works at: https://kijoms.uokerbala.edu.iq/home

 Part of the Atomic, Molecular and Optical Physics Commons, and the Plasma and Beam Physics Commons

## Recommended Citation

Fadhil, Hajir M.; Hassoon, Khaleel I.; and Salih, Hyder A. (2022) "Structural and Spectroscopic Analysis for Silver Bulk and Nanoparticles," *Karbala International Journal of Modern Science*: Vol. 8 : Iss. 2 , Article 5.
Available at: https://doi.org/10.33640/2405-609X.3220

This Research Paper is brought to you for free and open access by Karbala International Journal of Modern Science. It has been accepted for inclusion in Karbala International Journal of Modern Science by an authorized editor of Karbala International Journal of Modern Science. For more information, please contact abdulateef1962@gmail.com.

University of Kerbala

# Structural and Spectroscopic Analysis for Silver Bulk and Nanoparticles


## Abstract

In this research work, a pulsed Nd-YÅG laser having a wavelength of 1064 nm and energy (400-700 mJ (has been utilized as a source in an induced breakdown spectroscopy (LIBS) experiment to determine the density of electron and the tem-perature of Ag-plasma. Two forms of silver (as a bulk and as a compressed nano powder) have been used as targets in the LIBSs setup. The aim of the present work is to study the impact of target properties and laser energy on the plasma fea-tures formed by the interaction between a pulsed laser and these two forms of silver. The structural properties have been characterized via X-ray Diffraction (XRD), Scanning Electron microscopy (SEM) and Energy Dispersed X-Ray Spec-troscopy (EDX). For the two forms of silver, the electron density and the temperature increased with the laser energy rise from (400 mJ) to (700 mJ), and the Ag samples in the form of nano particles manifested enhanced LIBS signals. More-over, the LIBS technique can give complement information to other standard techniques for the material's diagnosis.



## Keywords

Ag Plasma, Ag NPs Plasma, X-ray diffraction, SEM, LIBS, EDS, Optical Emission Spectroscopy, Boltz-mann method, Stark broadening, Electron density, Electron temperature.



## Creative Commons License

This work is licensed under a Creative Commons Attribution-Noncommercial-No Derivative Works 4.0 License.



This research paper is available in Karbala International Journal of Modern Science: https://kijoms.uokerbala.edu.iq/home/vol8/iss2/5

ORIGINAL ARTICLE

# Structural and Spectroscopic Analysis for Silver Bulk and Nanoparticles

Hajir M. Fadhil*, Khaleel I. Hassoon, Hyder A. Salih

[a] Department of Applied Science, University of Technology, Baghdad, Iraq

**Abstract**

**In this research work, a pulsed Nd-Yag laser having a wavelength of 1064 nm and energy (400−700 mJ (has been utilized as a source in an induced breakdown spectroscopy (LIBS) experiment to determine the density of electron and the temperature of Ag-plasma. Two forms of silver (as a bulk and as a compressed nano powder) have been used as targets in the LIBSs setup. The aim of the present work is to study the impact of target properties and laser energy on the plasma features formed by the interaction between a pulsed laser and these two forms of silver. The structural properties have been characterized via X-ray Diffraction (XRD), Scanning Electron microscopy (SEM) and Energy Dispersed X-Ray Spectroscopy (EDX). For the two forms of silver, the electron density and the temperature increased with the laser energy rise from (400 mJ) to (700 mJ), and the Ag samples in the form of nano particles manifested enhanced LIBS signals. Moreover, the LIBS technique can give complement information to other standard techniques for the material's diagnosis.**

*Keywords:* Ag plasma, Ag NPs plasma, X-ray diffraction, SEM, LIBS, EDS, Optical emission spectroscopy, Boltzmann method, Stark broadening, Electron density, Electron temperature

## 1. Introduction

LIBS is a commonly used atomic emission spectroscopic method to analyze the physical and chemical properties of a variety of materials, such as metals, plastics, minerals, biological tissues, aerosols, liquids, and others [1,2]. Commonly, the LIBS technique uses one or more high-powered laser pulses to ablate a portion of the specimen surface, resulting in the production of temporary plasma [3]. The generated plasma consists of neutral atoms, ions and irradiation [4]. Properties of laser-created plasma are strongly influenced by a number of fundamental variables, including laser power, pulse duration, laser wavelength, and target material [5]. Also, LIBS is an interesting method when compared to many other methods of elemental analysis because of its fast reaction, high sensitivity, real-time, and noncontact properties [6]. In this technique, the emitted radiation is linked to the chemical composition of the sample and is monitored using a suitable detecting device (wavelength selector and detector) [3]. Also, the LIBS technique provides a number of advantages for sample analysis, including being fast, less damaging, cost-effective, and environmentally friendly, requiring little to no sample preparation, and allowing to a simultaneous multi-element detection [7]. It can be created as a durable and field portable [8]. Recently, LIBS has been utilized in a diversity set of applications, such as material analysis, ecological monitoring, forensic medicine, biological identification and even the description of fossils and the art works [9,10]. Researchers have attempted to develop LIBS technology, and they have lately utilized nano materials, which have become the focus of research because of their unique features from the bulk materials [11,12]. A solid-state Nd:YAG laser is typically employed for LIBS experiments because it is dependable, small, low-cost, and simple to use the source of laser pulses [13].

Received 29 September 2021; revised 26 January 2022; accepted 30 January 2022.
Available online 1 May 2022.

* Corresponding author at:
E-mail address: hajirmohammed66@gmail.com (H.M. Fadhil).

https://doi.org/10.33640/2405-609X.3220
2405-609X/© 2022 University of Kerbala. This is an open access article under the CC-BY-NC-ND license (http://creativecommons.org/licenses/by-nc-nd/4.0/).

Analysis of a bulk or a nanostructure material by LIBS provides important information that is complementary to various spectroscopic and microscopic methods, such as crystallite size, purity, and morphology. In the LIBS as a spectroscopic technique, the information that provides can be correlated with the other diagnosis techniques, such as the X-ray, Scanning Electron Microscopy, and Energy Dispersive X-ray. Unfortunately, despite the importance of LIBS, it is not used as much as X-ray diffraction (XRD) and SEM techniques.

In this article, LIBS technique is used along with XRD, SEM and EDS to investigate the physical properties of Ag as a bulk and as pressed nanoparticles.

There are various analytic methods to describe the laser-created plasma, including Thomson scattering, microwave and laser interferometry, photothermal beam deflection, Langmuir probe, laser induced fluorescence, mass spectroscopy, and optical emission spectroscopy [14]. The density of electron, the temperature of electron, the Debye length, and plasma frequency were calculated using optical emission spectroscopy (OES) [15].

## 2. Theoretical background

The Stark broadening of emission line can be employed to determine the density of electron from the full width at half maximum (FWHM) of the spectral line emission. The Stark wavelength broadening is given by [16]:

$$\Delta\lambda = 2\omega\left(\frac{N_e}{10^{16}}\right) + 3.5A\left(\frac{N_e}{10^{16}}\right)^{(1/4)}\left(1 - BN_D^{-1/3}\right)\omega\left(\frac{N_e}{10^{16}}\right) \quad (1)$$

where, A is a parameter for ion broadening, $N_e$ is the electron density, ω is the parameter of an electron impact or the Stark broadening value, B is a coefficient equivalent to (1.2) or (0.75) for ionic or neutral lines, and $N_D$ is the no. of particles that make the Debye sphere.

The ion broadening participation is so minor that it can be ignored. Consequently, the relationship between the broadening and electron density is abbreviated as [16]:

$$\Delta\lambda = 2\omega\left(\frac{N_e}{10^{16}}\right) \quad (2)$$

This formula is frequently used to calculate the $N_e$ of plasma generated from solid targets [17].

The electron temperature can be calculated from the Boltzmann's plot which is given by [18]:

$$\ln\left(\frac{\epsilon_{ji}\lambda_{ji}}{A_{ji}g_j}\right) = \frac{1}{KT}E_j + \ln\left(\frac{hcN_e}{Q(T)}\right) \quad (3)$$

where, $\varepsilon_{ji}$ is the emissivity ($W.m^{-3}$) or the intensity (I) of a spectral line, $A_{ji}$ is the probability of a transition ($s^{-1}$), $E_j$ is the energy (eV), $g_j$ is the upper level degeneracy, K is the Boltzmann's constant (eV. $K^{-1}$), T is the electron temperature, c is the speed of light ($ms^{-1}$), h is the Planck's constant (J.s), $N_e$ is the density of species ($m^{-3}$). The values are listed in Table 4, and Q(T) is the partition function of species usually taken as the statistical weight ($g_i$) of the ground state from the Atomic Spectral Database of the National Institute of Standards and Technology [19], and the values are listed in Table 3.

The Debye length for electrons in plasma is given by [20]:

$$\lambda_D = \sqrt{\frac{\epsilon_0 k_B T_e}{n_e e^2}} = 743\sqrt{\frac{T_e}{n_e}} \quad (4)$$

A basic equation for the electron plasma frequency (in hertz) is given by [21]:

$$f_{pe} = 8980\sqrt{n_e} \quad (5)$$

## 3. Experimental Part

Firstly, the silver nanoparticles (Ag NPs) having 40 nm size and 99.9% purity were pressed to a diameter of 1.5 cm and a thickness of 0.3 cm. The mass of silver powder (3 g) used as laser target during the experiment. The pressing was conducted using a hydraulic press under a pressure of 15 tons. Fig. (1) illustrates the shape of the silver nanopowder before and after pressing.

Secondly, the experimental setup of LIBS system in air is displayed in Fig. (2). The silver target was irradiated by Nd: YAG laser pulses (9 ns pulse period, 6 Hz repetition frequency, 2.2 mm spot size, and 1064 nm wavelength) with laser pulse energies: 400, 500, 600, and 700 mJ. An optical fiber with a photodetector was adjusted at 45° at 10 cm distance from the specimen in which the plasma was generated. The light emitted from the Ag plasma was

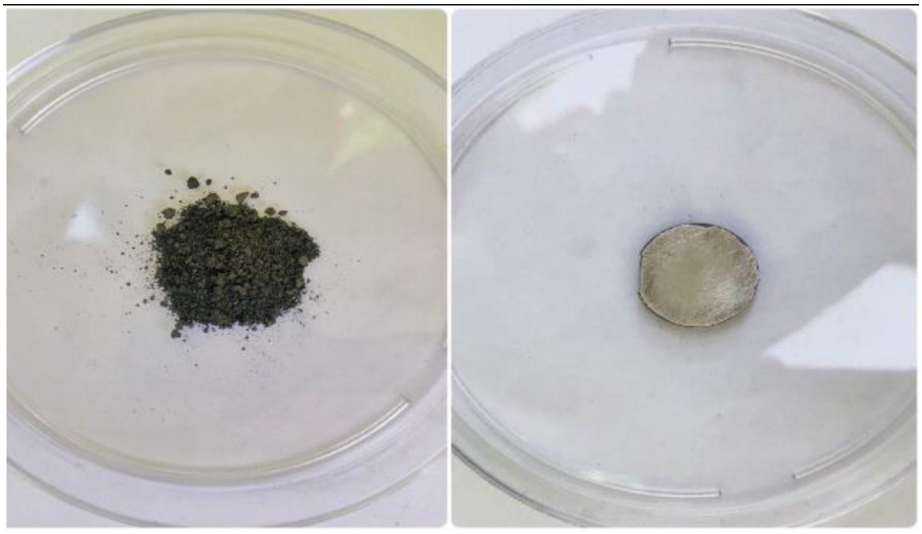

*Fig. 1. Two images of the silver nano powder before and after pressing.*

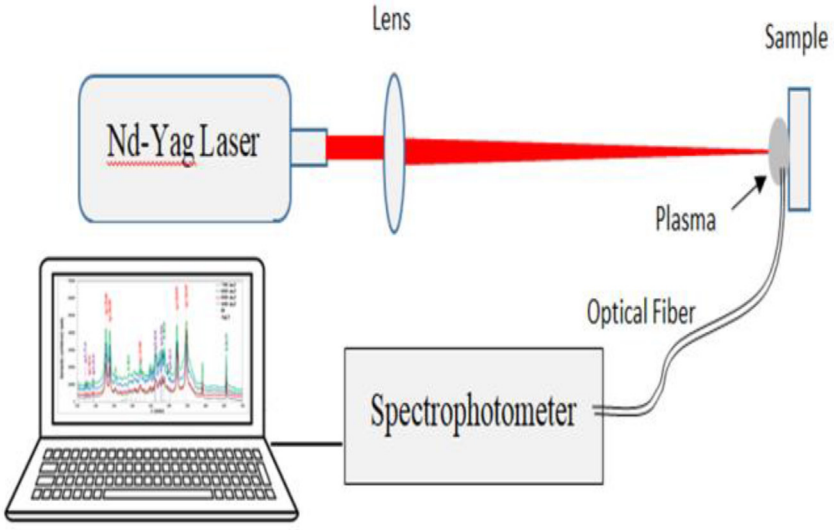


*Fig. 2. Schematic diagram of the LIBS experimental setup.*

analyzed using a spectrophotometer (Surwit, model S3000-UV-NIR). The data collected from that setup was utilized to calculate the electron temperature, electron density, plasma frequency, and the length of Debye length. The results were first discussed and then compared with a standard database from the National Institute of Standards and Technology [19].

The X-ray diffraction analysis was implemented using Shimadzu XRD 600C with source Cu-kα: $\lambda = 1.5418$ Å, Voltage: 40 kV, Current: 30 mA and scan range: 20–80 deg. The morphology of the surface was imaged by scanning electron microscope (ZEISS) with a high resolution showing a scale bar of 200 nm.

## 4. Results and discussions

### 4.1. X-ray diffraction

Both of the FWHM or $\beta$ and the peak position can be used to determine the average crystalline size with the use of Scherrer's equation [22]:

$$\mathbf{D}=\frac{0.9\,\boldsymbol{\lambda}}{\boldsymbol{\beta}\,\mathbf{cos}\theta} \tag{6}$$

where, $D$ is the average crystallite size, and $\theta$ is the Bragg angle (in degree) (see Table 1).

Figure (3a) evinces the XRD pattern of silver Ag NPs. The peaks were seen at angles 38.2°, 44.3°, 64.5° and 77.9° which can be assigned to diffraction from the planes (111), (200), (220) and (311), respectively. The results are presented in Table (1). In this table, the numbers were approximated to three significant figures. The highest intensity is at $2\theta = 38.2°$, and the crystal average size is around 13.6 nm. These results have a good agreement with references [23,24]. On the other hand, Figure (3b) elucidates the XRD diffraction patterns of silver as a bulk. The strongest four peaks are at $2\theta = 38.2°$, 44.3°, 64.5° and 77.9° and they are assigned to the orientations (111), (200), (220) and (311), respectively. The results are shown in Table 2. The highest intensity is at the angle $2\theta = 38.2°$, and the crystal average size of it is around 32.1 nm. These results are in agreement with Christy [25] and Meng [26].

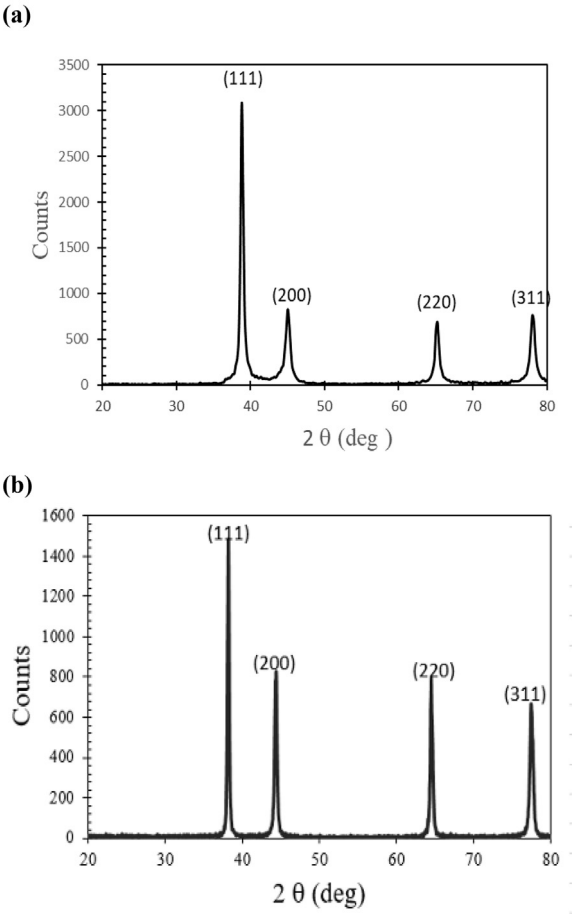


*Fig. 3. (a) XRD of silver nanoparticles. (b) X-ray diffraction patterns of silver bulk.*

### 4.2. Scanning electronic microscopy

SEM was employed to examine the particles surface shape as well as the size. Figure (4a) displays the scanning electronic microscopy image for Ag NPs with a scale bar of 200 nm. The image views the irregular particles shapes with some spherical-like shapes. The image J program has been used to calculate the average particle size of Ag NPs for the

*Table 1. X-ray diffraction peaks of Ag NPs.*

| Peak No. | 2θ (deg.) | Miller indices | β(deg.) | D (nm) | δ = 1/D2 ($cm^{-2}$) |
|---|---|---|---|---|---|
| 1 | 38.2° | (111) | 0.618 | 13.7 | 5.37E+11 |
| 2 | 44.3° | (200) | 0.8085 | 10.7 | 8.82E+11 |
| 3 | 64.5° | (220) | 0.7516 | 12.6 | 6.34E+11 |
| 4 | 77.9° | (311) | 0.7592 | 13.5 | 5.50E+11 |

*Table 2. X-ray diffraction peaks of Ag bulk.*

| Peak No. | 2θ (deg.) | Miller indices | β(deg.) | D (nm) | δ = 1/D2 ($cm^{-2}$) |
|---|---|---|---|---|---|
| 1 | 38.2° | (111) | 0.2626 | 32.1 | 9.73E+11 |
| 2 | 44.3° | (200) | 0.3308 | 26.0 | 1.48E+11 |
| 3 | 64.5° | (220) | 0.2774 | 33.9 | 8.69E+11 |
| 4 | 77.9° | (311) | 0.3642 | 28.0 | 1.28E+11 |

spherical-like shapes which is about 62 nm. Figure (4b) represents the SEM micrograph of pure Ag bulk. This figure obviously portrays that the Ag pellet consists of almost spherical grains. The average grain size is about 41 nm. The results are similar to reference [27].

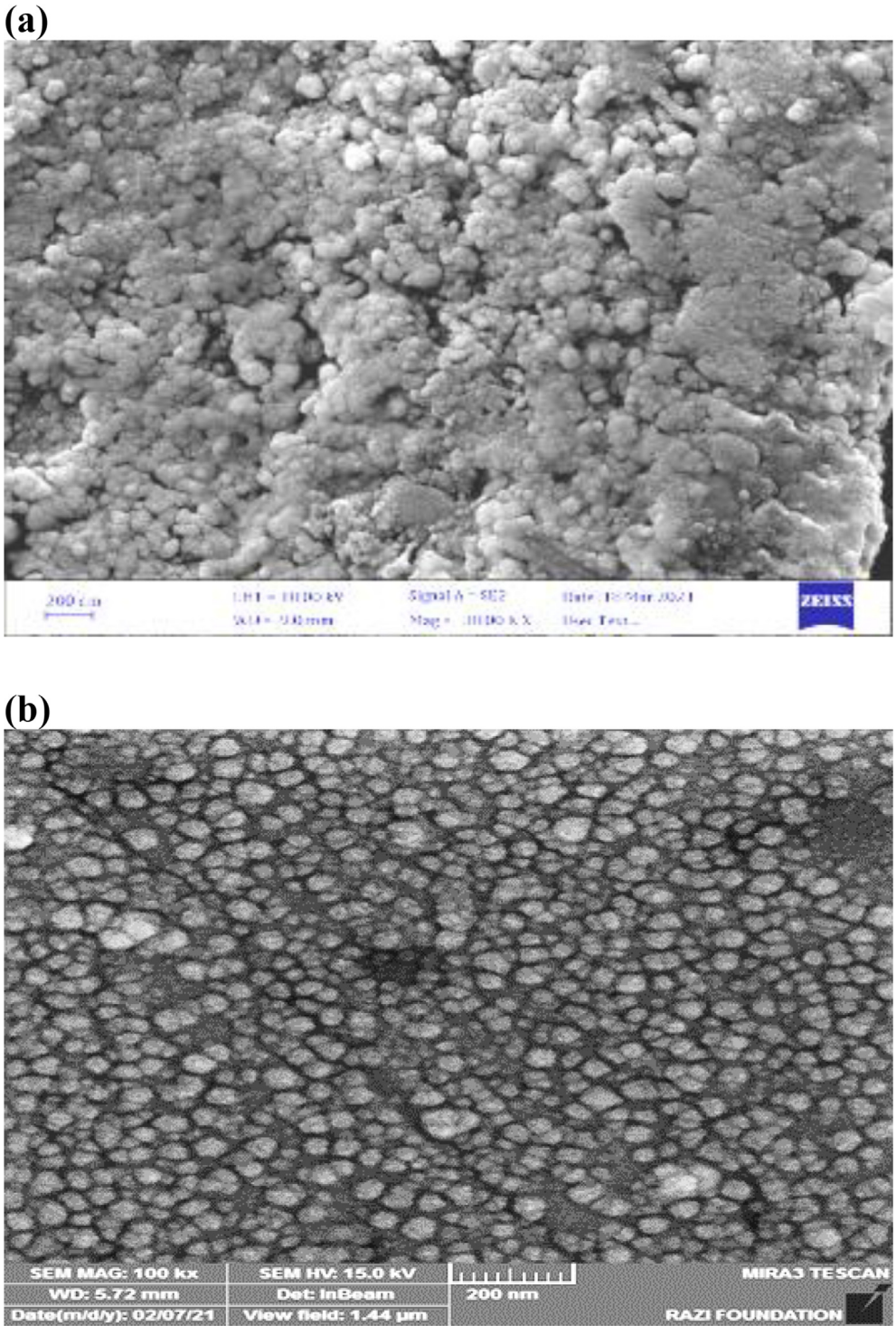


*Fig. 4. (a) Scanning electron micrographs of Ag NP (scale bar 200 nm). (b) Scanning electron micrographs of Ag bulk (scale bar 200 nm).*

### 4.3. Plasma emission analysis

#### 4.3.1. Emission spectrum of plasma for silver nanoparticles

Figure 5 reveals the emission spectrum of plasma for Ag NPs at atmospheric pressure in air for different pulse energies. In this figure, one can observe many peaks of Ag (I) at the wavelengths of 282.44, 328.07, 338.29, 421.10, 520.91 and 546.55 nm. The other peaks have been assigned to the ionic emission lines of Ag (II) at the wavelengths of 271.19, 293.40, 462, 478.84 and 502.73 nm. Furthermore, the higher laser energy has the higher intensity of emission. Also, the intensities of Ag (I) emission line are much higher than those of Ag (II). This is may be due to that the Ag (II) has higher ionization energy. This result agrees with the findings of reference [28].

#### 4.3.2. Emission spectrum of silver plasma

The emission spectrum of the Ag plasma of different laser energies at the atmospheric air pressure is shown in Figure (6). In this figure, there are many peaks of Ag (I) at the wavelengths of 328.07, 338.29, 421.10, 520.91 and 546.55 nm shown in the spectrum. The ionic emission lines of Ag (II) also appeared at the wavelengths of 271.19, 293.40, 462, 478.84 and 502.73 nm. All the intensities of peaks increase with the increasing of laser energy. Furthermore, based on the results that indicated in Figure (5), the total intensities of Ag (I) emission line are much higher than those of Ag (II). These results are in agreement with Abdul-Hassan [29].

The results demonstrate that the intensity of LIBS is higher for the nanostructured targets. This is due to that the surface to volume ratio for the Ag nanostructures is higher than that for the bulk structure. Also, the roughness of Ag NPs is higher and this leads to lower reflectivity and hence higher absorption.

Table 3 lists the spectroscopic parameters from (NIST database).

Table 4 lists the results of the calculations of the temperature of electron ($T_e$), FWHM, density of electron ($n_e$), frequency of plasma ($f_p$), and length of Debye ($\lambda_D$) for Ag bulk and Ag NPs targets at different laser energies by the Boltzmann's method and Stark broadening that can be calculated using the intensity ratio of the spectral lines of the atom or ion of the same ionization stage. All of the computed plasma parameters ($\lambda_D$ and $f_p$) satisfied the requirements of plasma. Because $f_p$ is proportional to $n_e$, this depicts that the $f_p$ increases with the laser energy.

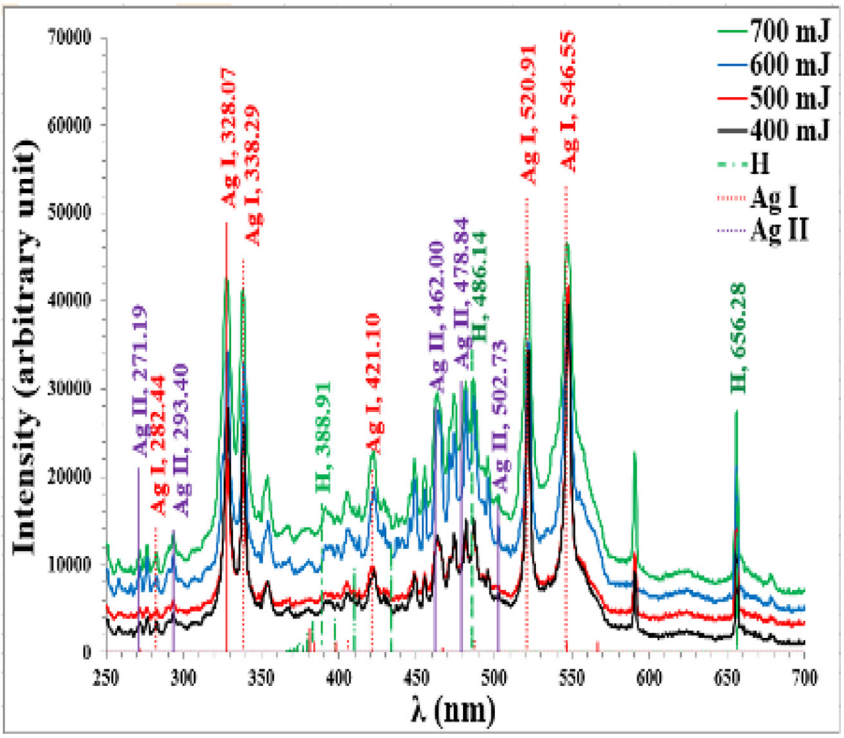


*Fig. 5. Emission spectra of laser induced Ag NPs target with different laser energies.*

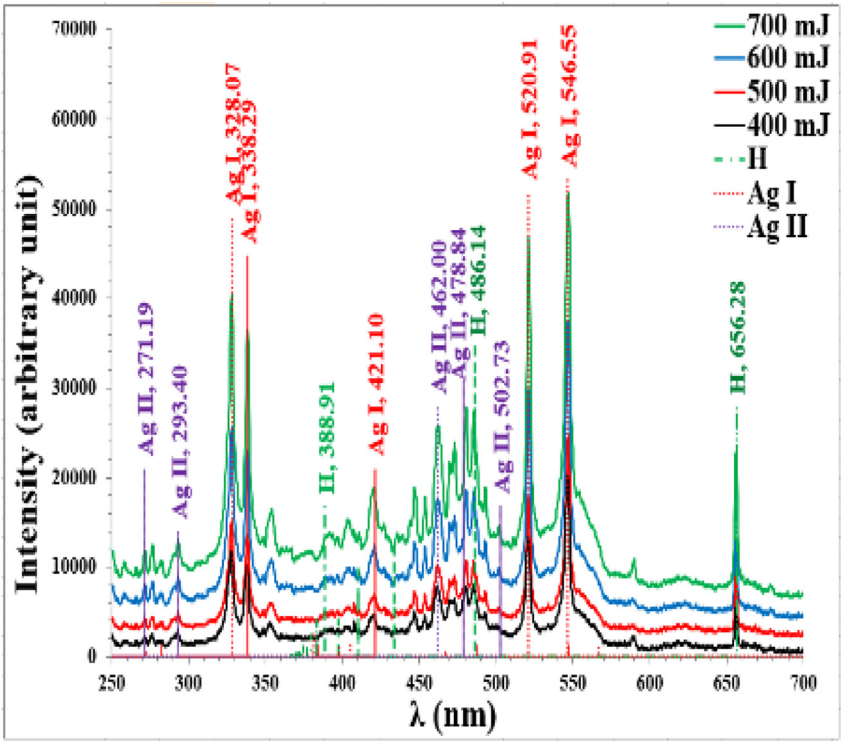


*Fig. 6. Emission spectra of laser induced Ag target with different laser energies.*

*Table 3. Spectroscopic parameters of Ag I and Ag II that taken from reference [19].*

| ion | λ (nm) | $g_i$ | $g_j$ | $A_{ji}$-gj ($s^{-1}$) | Ei (ev) | Ej (ev) | FWHM |
|---|---|---|---|---|---|---|---|
| Ag | 328.07 | 2 | 4 | 5.60E+08 | 0 | 3.778 | 1.400 |
| I | 338.30 | 2 | 2 | 2.60E+08 | 0 | 3.664 | 1.550 |
| | 520.91 | 2 | 4 | 3.0DE+08 | 3.664 | 6.043 | 1.600 |
| | 546.55 | 4 | 6 | 5.2DE+08 | 3.778 | 6.046 | 1.650 |
| | 547.15 | 4 | 4 | 5.60E+07 | 3.778 | 6.043 | 1.700 |
| Ag | 271.19 | 9 | 7 | 1.40E+09 | 10.374 | 14.944 | 1.800 |
| II | 293.40 | 7 | 7 | 5.00E+08 | 10.711 | 14.944 | 1.900 |
| | 462.00 | 7 | 5 | 1.00E+06 | 11.051 | 13.734 | 2.000 |
| | 478.84 | 3 | 5 | 4.80E+06 | 11.146 | 13.734 | 2.050 |
| | 502.73 | 5 | 5 | 1.70E+06 | 11.268 | 13.734 | 2.100 |

*Table 4. Plasma parameters for Ag NPs and Ag bulk with different laser energies.*

| E (mJ) | $T_e$ (ev) | $n_e$*$10^{16}$ ($cm^{-3}$) | $f_p$ *$10^{12}$ (Hz) | $\lambda_D$ *$10^{-6}$ (cm) |
|---|---|---|---|---|
| | **Ag NPs** | | | |
| 400 | 0.299 | 39.645 | 5.654 | 0.645 |
| 500 | 0.331 | 46.049 | 6.094 | 0.630 |
| 600 | 0.361 | 48.251 | 6.238 | 0.642 |
| 700 | 0.387 | 50.486 | 6.381 | 0.650 |
| | **Ag bulk** | | | |
| 400 | 0.150 | 5.738 | 2.151 | 1.200 |
| 500 | 0.154 | 6.213 | 2.238 | 1.170 |
| 600 | 0.158 | 6.700 | 2.324 | 1.141 |
| 700 | 0.160 | 6.948 | 2.367 | 1.126 |

#### 4.3.3. Influence of Ag metal on the electron temperature

The electron temperature ($T_e$) for Ag and Ag NPs plasmas that generated by laser at the atmospheric pressure can be obtained from the slope of equation (3). The atomic lines of Ag (I) and Ag NPs (I) elements have been used to calculate the electron temperature at various laser energies (400, 500, 600 and 700 mJ). By using NIST data [19] and equation (3), the electron temperatures have been calculated which are presented in Table (4) and shown in Figure (7). This figure manifests many features, where the temperature of the electron of both plasmas increases with the energy of laser increase. These results are in agreement with references [30–32]. The value of the electron temperature of Ag NPs plasma is greater than that of the Ag bulk plasma under the same conditions. The reason behind that is the rise in the penetration depth of the nano materials laser energy as well as the big surface area of such materials, which permit to further energy transfer inside the nano material in addition to the elevated temperature of the plasma created from it [10].

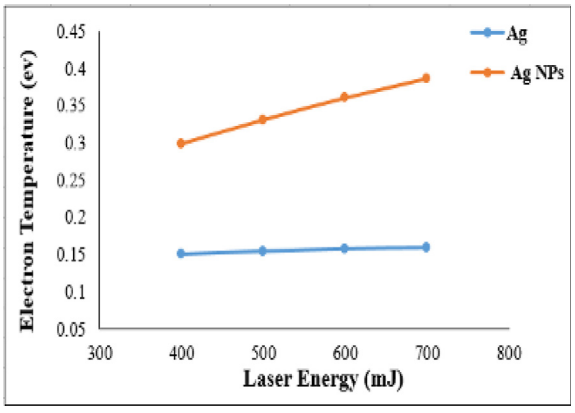


*Fig. 7. The variation of electron temperature with laser energy in Ag bulk and Ag NP plasmas at atmospheric pressure.*

#### 4.3.4. Influence of Ag metal on the electron density

According to equation (2) and NIST data [18], the impact of laser energy on the electron density of Ag and Ag NP plasmas is evinced in Figure (8). It can be seen in this figure, the electron density of both plasmas increases at different rates depending on the laser energy increasing [33]. More exciting species, such as ions and free electrons, are generated as the laser radiance increases. The electron density of the Ag NPs target is larger than that of the Ag bulk target at the same laser energy due to the quantum mechanical behavior of the nano materials.

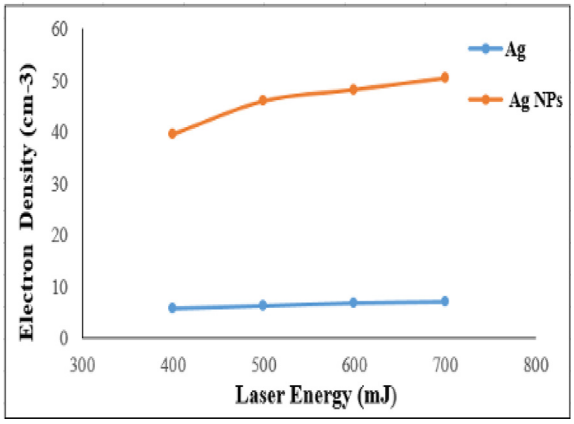


*Fig. 8. The variation of electron density with laser energy for Ag and Ag NP plasmas.*

#### 4.3.5. Effect of Ag metal on the plasma frequency

The variation of electron frequency with the laser energy of Ag and Ag NP plasmas is portrayed in Figure (9) using equation (5). In this figure, the data points exhibit the increasing of the plasma frequency with the increasing of laser energy for the both plasmas. This behavior resulted in by the increase of the electron concentration with an increase in the energy of laser, and this caused a rise in the plasma frequency. The result showed that the value of plasma frequency in the Ag NP plasma is greater than that in the Ag plasma.

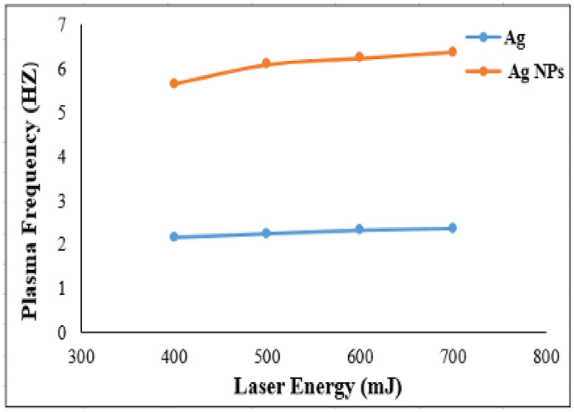


*Fig. 9. The variation of plasma frequency with laser energy of Ag and Ag NP plasmas.*

### 4.4. Energy Dispersed X-Ray Spectroscopy (EDX)

Figure (10a) manifests the Ag NP analysis by EDX, and Figure (10 b) shows the Ag bulk analysis by EDX. The relative peak heights of the observed Ag particles have been clearly seen at 3 keV due to the surface plasma resonance. For the spectral signals

for carbon, cadmium and oxygen, the peak for C has been noted (at 0.3 keV), Cd (at 3.1 keV) and $O_2$ (at 0.5 keV). This indicates that these elements have been absorbed on the surface of the samples. The peak of $O_2$ has been elucidated at (0.5 keV), which might be ascribed to the existence of the surface silver oxide. These results are in agreement with Ahluwalia et al. [34] and Li et al. [35]. The difference between the nanomaterial and bulk has been noticed only in terms of the intensity, where the intensity of the nanomaterial is greater than the bulk.

Through the results, it was found that in the LIBS technique, the number of peaks obtained from LIBS is more than the number of peaks resulted from EDS. Also, LIBS has a higher sensitivity than EDS to know the components of materials and study their properties.

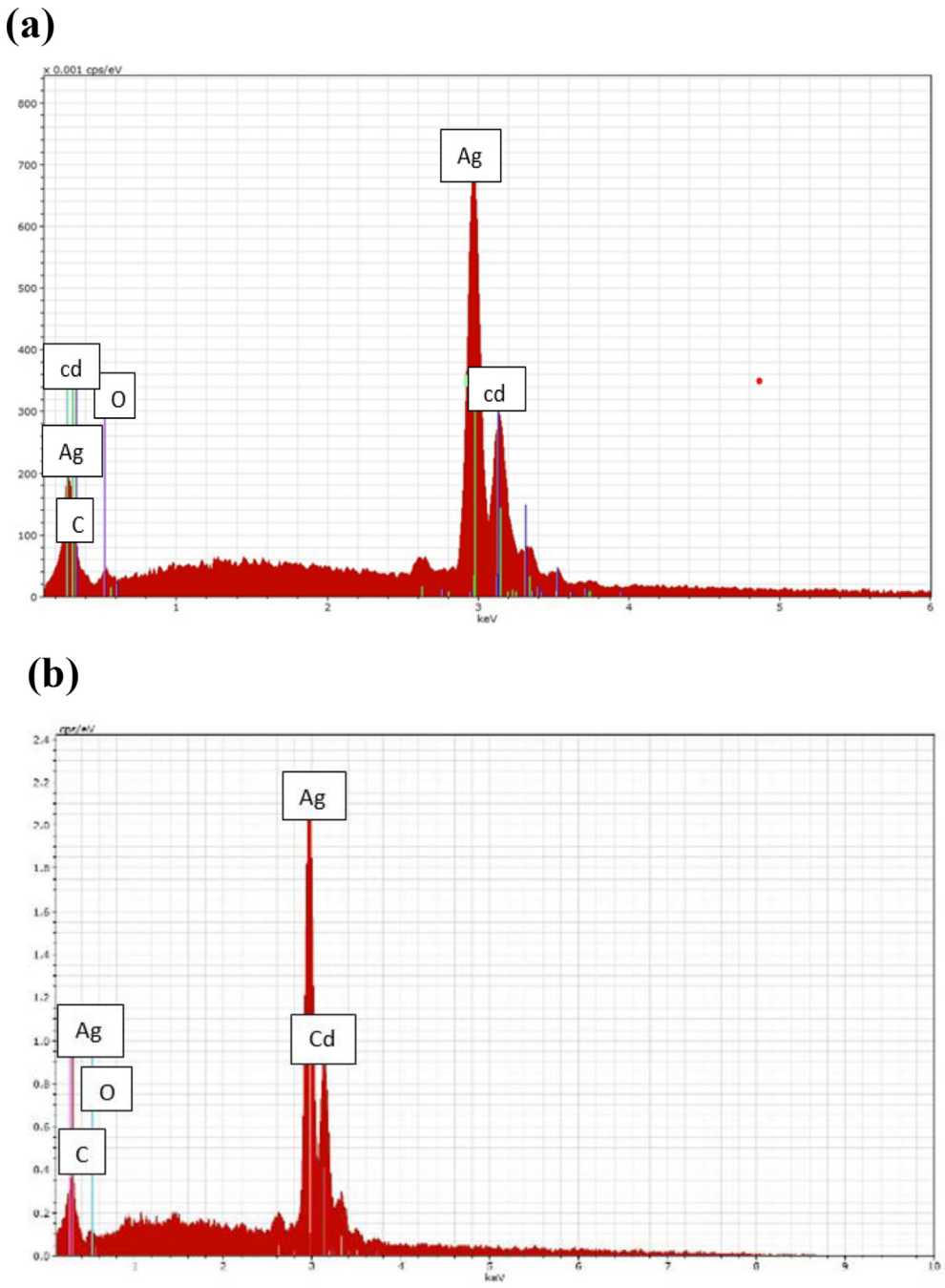


*Fig. 10. (a) EDS of Ag NP. (b) EDS of Ag bulk.*

## 5. Conclusions

Two forms of silver samples were used as targets in laser breakdown induced spectroscopy (LIBS). In conclusion, for the purpose of LIBS diagnosis, it's recommended to use samples in form of nanoparticles. The LIBS technique can give complement information to the other standard techniques for the material diagnosis.

## References


[1] S. Musazzi, U. Perini, Laser-induced breakdown spectroscopy: theory and applications, in: S. Musazzi, U. Perini (Eds.), Springer series in optical sciences, Springer, Berlin, Heidelberg, 2014, pp. 59–89, https://doi.org/10.1007/978-3-642-45085-3_3.

[2] N.M. Saadoon, N.M. Hadi, S.H. Sabeeh, Diagnosis of copper plasma by laser induced breakdown spectroscopy, IOP Conf Ser Mater Sci Eng 757 (2020) 1–8, https://doi.org/10.1088/1757-899x/757/1/012023.

[3] J. Feng, Z. Wang, Z. Li, W. Ni, Study to reduce laser-induced breakdown spectroscopy measurement uncertainty using plasma characteristic parameters, Spectrochim Acta Part B: At Spectrosc 65 (2010) 549–556, https://doi.org/10.1016/j.sab.2010.05.004.

[4] A.M. El Sherbini, A.A.S. Al Aamer, Measurement of plasma parameters in laser-induced erbreakdown spectroscopy using Si-lines, World J Nano Sci Eng 2 (2012) 206–212, https://doi.org/10.4236/wjnse.2012.24028.

[5] S.H. Sabeeh, K.A. Ali, Conversion efficiency of laser-produced Sn plasma, in: The pro. 4th Int. Sci. Conf. of Salahaddin Univ., Erbil. 2, 2011, pp. 801–803.

[6] Z.Z. Wang, Y. Deguchi, M. Kuwahara, J.J. Yan, J.P. Liu, Enhancement of laser-induced breakdown spectroscopy (LIBS) detection limit using a low-pressure and short-pulse laser-induced plasma process, Appl Spectrosc 67 (2013) 1242–1251, https://doi.org/10.1366/13-07131.

[7] X. Xu, C. Du, F. Ma, Y. Shen, J. Zhou, Fast and simultaneous determination of soil properties using laser-induced breakdown spectroscopy (Libs): a case study of typical farmland soils in China, Soil Syst 3 (2019) 1–18, https://doi.org/10.3390/soilsystems3040066.

[8] F.C. De Lucia Jr., R.S. Harmon, K.L. McNesby, R.J. Winkel Jr., A.W. Miziolek, Laser-induced breakdown spectroscopy analysis of energetic materials, Appl Opt 42 (2003) 6148–6152, https://doi.org/10.1364/AO.42.006148.

[9] T.A. Labutin, A.M. Popov, V.N. Lednev, N.B. Zorov, Correlation between properties of a solid sample and laser-induced plasma parameters, Spectrochim Acta - Part B: At Spectrosc 64 (2009) 938–949, https://doi.org/10.1016/j.sab.2009.07.033.

[10] A.J. Effenberger Jr., J.R. Scott, Effect of atmospheric conditions on LIBS spectra, Sensors 10 (2010) 4907–4925, https://doi.org/10.3390/s100504907.

[11] Y.A. Ali, R.A. Khamis, Spectroscopic study of copper plasma produced by Nd: YAG laser from the nano and bulk copper targets, J Phys Conf Ser 1818 (2021) 1–9, https://doi.org/10.1088/1742-6596/1818/1/012008.

[12] A. k AL-Ogaili, A.K. Ali, T.H. Ali, Preparation of silver nanoparticles and study the optical and antibacterial properties, Eng Tech J 33 (2015) 478–487.

[13] V. Lednev, S.M. Pershin, A.F. Bunkin, Laser beam profile influence on LIBS analytical capabilities: single vs. multimode beam, J Anal At Spectrom 25 (2010) 1745–1757, https://doi.org/10.1039/C0JA00017E.

[14] S.S. Harilal, C.V. Bindhu, M.S. Tillack, F. Najmabadi, A.C. Gaeris, Internal structure and expansion dynamics of laser ablation plumes into ambient gases, J Appl Phys 93 (2003) 2380–2388, https://doi.org/10.1063/1.1544070.

[15] M.G. Jasim, Q.A. Abbas, Influence of working pressure and lasing energy of Al plasma in laser-induced breakdown spectroscopy, Iraqi J Phys 17 (2019) 59–66, https://doi.org/10.30723/IJP.V17I40.406.

[16] S. Duixiong, S. Maogen, D. Chenzhong, W. Guanhong, C. Xiangnian, A comparative study of the laser induce breakdown spectroscopy in single- and double-pulse laser geometry, Plasma Sci Technol 16 (2013) 26–36, https://doi.org/10.1088/1009-0630/16/4/13.

[17] W.A. Farooq, W. Tawfik, F.N. Al-Mutairi, Z.A. Alahmed, Qualitative analysis and plasma characteristics of soil from a desert area using LIBS technique, J Opt Soc Korea 17 (2013) 548–558, https://doi.org/10.3807/JOSK.2013.17.6.548.

[18] J.A. Aguilera, C. Aragón, Characterization of a laser-induced plasma by spatially resolved spectroscopy of neutral atom and ion emissions: comparison of local and spatially integrated measurements, Spectrochim Acta - Part B At Spectrosc 59 (2004) 1861–1876, https://doi.org/10.1016/J.SAB.2004.08.003.

[19] NIST Atomic Spectra Database. https://doi.org/10.18434/T4W30F/pml/atomic-spectra-database/ (accessed 3 13,2022).

[20] P. Gibbon, Introduction to plasma physics, CAS-CERN Accel Sch Plasma Wake Accel 1 (2020) 1–19, https://doi.org/10.5170/CERN-2016-001.51.

[21] D.A. Gurnett, A. Bhattacharjee, Introduction to plasma physics: with space and laboratory applications, Cambridge univ. press, Harlow, NY, 2005, https://doi.org/10.5860/choice.43-0375.

[22] S.J. Hashim, K.I. Hassoon, O.N. Salman, Structural properties of Fe doped $TiO_2$ nanorods prepared by low cost hydrothermal method, Eng Technol J 38 (2020) 177–183, https://doi.org/10.30684/ETJ.V38I3B.1800.

[23] A.S. Hassanien, U.T. Khatoon, Synthesis and characterization of stable silver nanoparticles, Ag-NPs: discussion on the applications of Ag-NPs as antimicrobial agents, Phys B Condens Matter 554 (2019) 21–30, https://doi.org/10.1016/J.PHYSB.2018.11.004.

[24] A.A. Mostafa, S.R.M. Sayed, E.N. Solkamy, M. Khan, M.R. Shaik, A. Al-Warthan, et al., Evaluation of biological activities of chemically synthesized silver nanoparticles, J Nanomater 16 (2015) 1–7, https://doi.org/10.1155/2015/789178.

[25] A.J. Christy, M. Umadevi, Synthesis and characterization of monodispersed silver nanoparticles, Adv Nat Sci Nanosci Nanotechnol 3 (2012) 1–4, https://doi.org/10.1088/2043-6262/3/3/035013.

[26] Y. Meng, A sustainable approach to fabricating ag nanoparticles/PVA hybrid nanofiber and its catalytic activity, Nanomaterials 5 (2015) 1124–1135, https://doi.org/10.3390/nano5021124.

[27] M. Vanaja, G. Annadurai, Coleus aromaticus leaf extract mediated synthesis of silver nanoparticles and its bactericidal activity, Appl Nanosci 3 (2013) 217–223, https://doi.org/10.1007/s13204-012-0121-9.

[28] G.A. Kahrilas, L.M. Wally, S.J. Fredrick, M. Hiskey, A.L. Prieto, J.E. Owens, Microwave-assisted green synthesis of silver nanoparticles using orange peel extract, ACS Sustain Chem Eng 2 (2014) 367–376, https://doi.org/10.1021/SC4003664.

[29] I.A. Abdul-hassan, A.K. Abbas, I.M. Ibrahim, Plasma characteristics of Ag and Cu metals produced by pulse laser ablation of Nd : YAG laser in air, J Recent Res Appl Stud 5 (2018) 1–6.

[30] I. Rehan, K. Rehan, S. Sultana, M. Oun ul Haq, M.Z.K. Niazi, R. Muhammad, Spatial characterization of red and white skin potatoes using nano-second laser induced breakdown

in air, Eur Phys J Appl Phys 73 (2016) 1–8, https://doi.org/10.1051/epjap/2015150453.
[31] I. Rehan, M. Zubair Khan, I. Ali, K. Rehan, S. Sultana, S. Shah, Spectroscopic analysis of high protein nigella seeds (Kalonji) using laser-induced breakdown spectroscopy and inductively coupled plasma/optical emission spectroscopy, Appl Phys B 124 (2018) 1–8, https://doi.org/10.1007/s00340-018-6915-z.
[32] A.M. Popov, S.M. Zaytsev, I.V. Seliverstova, A.S. Zakuskin, T.A. Labutin, Matrix effects on laser-induced plasma parameters for soils and ores, Spectrochim Acta - Part B: At Spectrosc 148 (2018) 205–210, https://doi.org/10.1016/j.sab.2018.07.005.
[33] H.A. Salih, N. Yassoob A, S.N. Mazhir, Relativistic self-focusing of intense laser beam in magnetized plasma, Eng Tech J 32 (2014) 849–861.
[34] V. Ahluwalia, J. Kumar, R. Sisodia, N.A. Shakil, S. Walia, Green synthesis of silver nanoparticles by Trichoderma harzianum and their bio-efficacy evaluation against Staphylococcus aureus and Klebsiella pneumonia, Ind Crop Prod 55 (2014) 202–206, https://doi.org/10.1016/j.indcrop.2014.01.026.
[35] X. Li, H. Li, Y. Chen, X. Zeng, Silver conductor fabrication by laser direct writing on $Al_2O_3$ substrate, Appl Phys A 79 (2004) 1861–1864, https://doi.org/10.1007/s00339-004-2914-5.